Chapter 11

Progress in Theoretical and Numerical Tools Devoted to Understanding of Acoustic Devices Behavior

T. Laroche and S. Ballandras

Additional information is available at the end of the chapter

http://dx.doi.org/10.5772/56164

1. Introduction

Since several decades, the acoustic devices improvement depends largely on the theoretical and Numerical tools. In Acoustic domain, the simulations provide results in high agreement with the measurements. The numerical methods mainly used are either heuristic or algorithmic. The heuristic ones give results rapidly but not necessary optimized e.g. the Mixed Matrix formulation [1–3]. The second kind of numerical methods (algorithmic ones) requires advanced mathematical development and also complex numerical algorithms e.g. Finite Element Analysis (FEA)/Boundary Element Method (BEM) [4]. FEA also provides the data structures for the heuristic methods such as P-Matrix method. In this chapter, we go over the second kind of numerical methods i.e. the exact ones (FEA/BEM). First, the basis equations are detailed as well as the current level of the numerical tools (Periodic FEA/BEM [5]). Next, FEA improvements are demonstrated. Indeed, new research fields in acoustic need to consider extra configurations which cannot be treated by the periodic way e.g. in dual-mode SAW filters [6]. So, a non-periodic model was developed and implemented. The theoretical approach is identical to the one used in periodic case. The strategy of digitizing is also the same i.e. So only the inhomogeneous part of the studied configuration must be discretized. By contrast, the surrounding space is considered by using boundary conditions. Indeed, an acoustic devices is not flying in a free space but if one does not take care of the boundary that is exactly what it is simulate. The edges of the mesh used in a FEA act as a perfect mirror. So, without boundary conditions the component is in the vacuum. This remark is valid both for the non-periodic and periodic. To avoid any problems with the bottom and top limits of the mesh, one must first develop a BEM to simulate the radiation in a multilayered substrate or surrounding medium. Here, BEM is based on Green functions. The inverse Green problem is solved for the periodic case [7] while the direct one is used for the non-periodic systems [8]. In a second step the artificial reflexions on the side edges of the meshed grid must be eliminated. In periodic configuration (e.g. SAW transducers), this

is considered by using periodic conditions on the edges [9]. In non-periodic case, a Perfectly Matched Layer (PML) method must be used and specially for spatially finite SAW resonators. This method avoids artificial reflexions on the edge side of the meshed.

This work presents first the basis of the FEA with a brief state of the art in simulation with the main known results until now both for the non-periodic and periodic cases. Next, the last improvements applied to these numerical investigations are introduced. The boundary conditions are mainly developed to address new configurations such as the spatially finite SAW devices. The radiation problem (BEM) is first shown and secondly the PML. The last part is dedicated to the new results obtained by using the latter improvements.

2. Analytical recipes and state of the art

2.1. Fundamental equations

The Finite Element model allows to simulate the behavior of acoustic devices against many parameters such as coated medium, electrodes apodization... This method was first initiated by Tiersten [10]. The principle consists in the equilibrium of the potential and kinetic energy in the volume with the electrical and mechanical excitation applied on the edges. Thus we obtained the variational formulation from the equilibrium point of the Lagrangian functional [11] :

$$\begin{aligned}&\iiint_\Omega \left(\frac{\partial \delta u_i}{\partial x_j} C_{ijkl} \frac{\partial u_l}{\partial x_k} + \frac{\partial \delta u_i}{\partial x_j} e_{kij} \frac{\partial \phi}{\partial x_k} + \frac{\partial \delta \phi}{\partial x_i} e_{ijk} \frac{\partial u_j}{\partial x_k} - \frac{\partial \delta \phi}{\partial x_j} \varepsilon_{jk} \frac{\partial \phi}{\partial x_k} - \rho\omega^2 u_i \delta u_i\right) dV = \\ &\iiint_\Omega F_i \delta u_i dV + \iint_\Gamma \delta u_i T_{ij} n_j dS + \iint_\Gamma \delta\phi D_j n_j dS\end{aligned} \tag{1}$$

u_i and ϕ are respectively the displacement and the potential unknowns, C_{ijkl} the elastic constants, e_{ijk} the piezoelectric ones, ρ the density and ε_{ij} the dielectric coefficients. F_i, T_{ij} and D_i are respectively the forces the stress and the displacement vector. Ω and Γ are respectively the studied domain and its frontier with the outer space (See Fig. 1). The solution of such an equation is not trivial. The scheme of FEA allows to find a global solution from an exact one computed at local points. The global solution is obtained by polynomial interpolation in finite elements. The sum of each elements give the Ω domain. The variational equation (1) is given for the FEA scheme:

$$\begin{aligned}&\sum_{e=1}^{E} \iiint_{\Omega^{(e)}} \left(\frac{\partial \delta u_i^{(e)}}{\partial x_j} C_{ijkl}^{(e)} \frac{\partial u_l^{(e)}}{\partial x_k} + \frac{\partial \delta u_i^{(e)}}{\partial x_j} e_{kij}^{(e)} \frac{\partial \phi^{(e)}}{\partial x_k} + \frac{\partial \delta \phi^{(e)}}{\partial x_i} e_{ijk}^{(e)} \frac{\partial u_j^{(e)}}{\partial x_k}\right. \\ &\left. - \frac{\partial \delta \phi^{(e)}}{\partial x_j} \varepsilon_{jk}^{(e)} \frac{\partial \phi^{(e)}}{\partial x_k} - \rho\omega^2 u_i^{(e)} \delta u_i^{(e)}\right) dV = \\ &\iiint_{\Omega^{(e)}} F_i^{(e)} \delta u_i^{(e)} dV + \iint_{\Gamma^{(e)}} \delta u_i^{(e)} T_{ij}^{(e)} n_j^{(e)} dS + \iint_{\Gamma^{(e)}} \delta\phi^{(e)} D_j^{(e)} n_j^{(e)} dS\end{aligned} \tag{2}$$

where e defines the e^{th} element and E the total number of elements. In equation (2), all the unknowns (δu, u...) should be written using polynomial interpolation for each element [12]. Each quantities $\Delta^{(e)}(x_i)$ is written according to the following interpolation in one element:

$$\Delta^{(e)}(x_i) = \sum_{n=1}^{N_e} \Delta^{(e,n)} P^{(e,n)}(x_i), \tag{3}$$

where x_i is one space direction, N_e the number of nodes in the e^{th} element, $\Delta^{(e,n)}$ the value of the quantity Δ at the nth node of the eth element and $P^{(e,n)}(x_i)$ is the Lagrangian interpolation polynomial for the same node. For the sake of clarity, only the elastic part is written below according to the FEA formulation for a dimensional device (for instance along x_1 in Fig. 1) with all the mechanical contributions:

$$\sum_{e=1}^{E}\sum_{n=1}^{N_e}\sum_{\mu=1}^{N_e}\left(\iiint_{\Omega^{(e)}}\frac{\partial P^{(e,n)}(x_1)}{\partial x_1}C_{i11l}^{(e)}\frac{\partial P^{(e,\mu)}(x_1)}{\partial x_1}dV - \rho\omega^2\iiint_{\Omega^{(e)}}P^{(e,n)}(x_1)P^{(e,\mu)}(x_1)dV\right)u_i^{(e,\mu)}\delta u_i^{(e,n)} = 0. \tag{4}$$

In the nodal expression (4), the right hand is zero. The boundary is actually not considered in this trivial model.

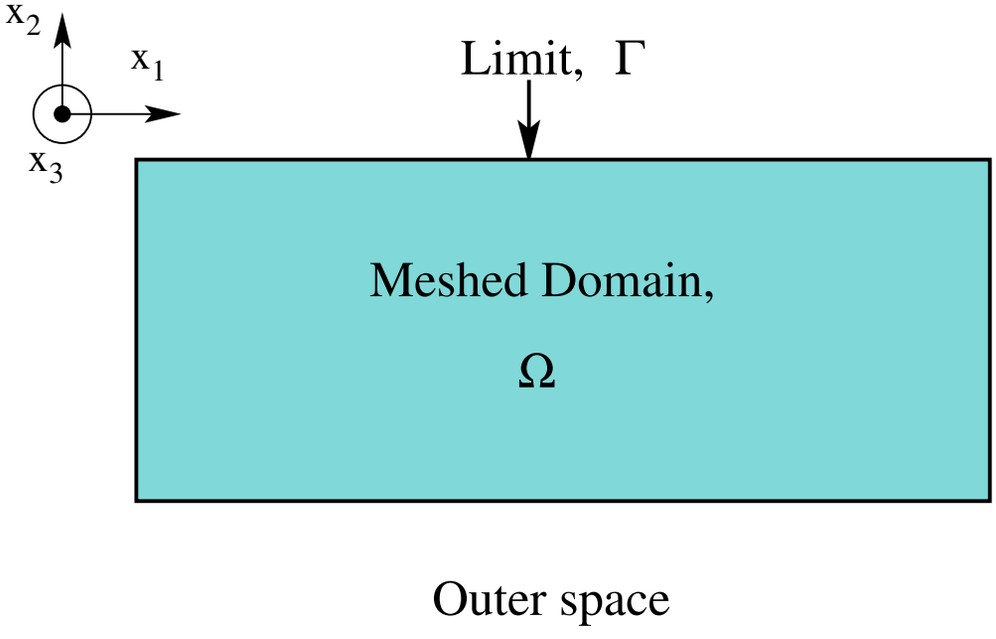

Figure 1. Splitting of space for a FEA. Ω is the inhomogeneous space under simulation. This is the meshed domain in which the FEA is applied. Γ is the boundary of Ω with the remaining space. The latest is either simulated using boundary conditions or considered as vacuum.

The right hands of equations (1) and (2) show several boundary conditions. They are represented by the integration on the limit Γ. This domain is also discretized in all its elements. The boundary conditions can be applied on each element considering a condition on the stress as well as on the displacement or the potential. These parts are for example the beginning of the radiating conditions. We define below this condition and how consider it in the variational equation.

2.2. State of the art

The FEA is known since forty years in piezoelectric problem [13]. However, the finite dimension of the meshed space involves the problem of the spurious reflexions on the edges. Indeed, by default the edges act as perfect mirrors. The device is seldom in the vacuum.

Moreover, to consider a real case, the device must be supported by a substrate. So, the boundary conditions have to be set by considering all these constraints.

First, we were interested in the periodic acoustic devices e.g. Surface Acoustic Waves devices (SAW). So, the side edges constraints were easily avoided. Indeed, periodic condition was set on them [14]. to consider realistic case, the radiating medium must be modeled. The mix of FEA and BEM in periodic configuration was so implemented [15]. A lot of results with high accuracy are obtained from this numerical method. One of these results is depicted in figure 2 and 3. These results come from Ref. [15]. This is the comparison between experimental results

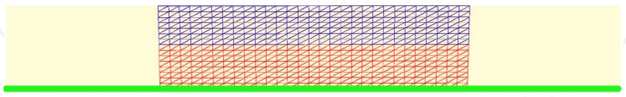

Figure 2. Mesh of the considered prominent electrode grating device Ref. [16] red part of the mesh: quartz; blue part: Al; and green section: interface between FEA and BEM.

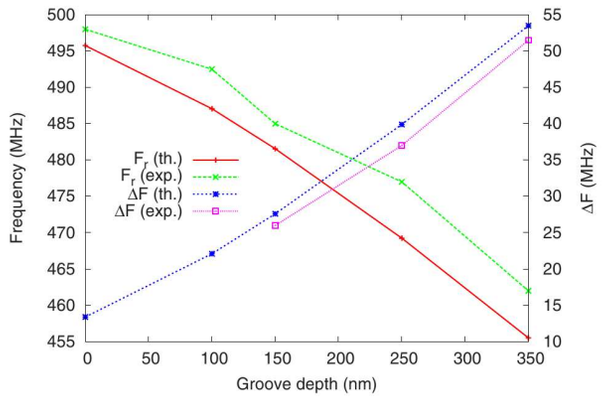

Figure 3. Comparison between theoretical and experimental resonance frequency and stop bandwidth for prominent electrode grating based resonators Ref [16].

(Ref. [16]) and numerical simulations combining both FEA and BEM for Surface Transverse Wave problem under massive electrodes. In that case, the grating's period was 5 m with a metalization ratio of 0.5. The strip height atop the resulting prominent quartz ridge was 300 nm with a groove depth ranging from 0 to 350 nm. FEA/BEM approach. The typical mesh for prominent electrode gratings is plotted in Fig. 2. Both the resonance frequency and frequency stop-band width were measured. The comparison between FEA results and experiments are reported in figure 3. It highlights a good prediction of the behavior of the device.

3D periodic problems have also be considered. We depict here a very original work on a two direction a 2D periodic transducer consisting of square dots or pads exhibiting a double excitation potential alternation (along x1 and x2, here the axes defining the surface) [17]. In other words, a two directions SAW resonator is investigated in this previous paper.We particularly focused on one excitation configuration consisting in potential alternation along both period d1 and d2 as illustrated in figure 4. It is however clear that the actual implementation of such an excitation configuration is quite difficult to achieve, as we can not imagine the fabrication of metal bridges for accessing all the square dots of the surface. We then imagine the use of a dielectric spacer allowing for preventing the presence of electrical charge at the surface between the dots but allowing for the connection we are looking for. This

is graphically illustrated in figure 5, showing an example of mesh. This kind of mesh has been

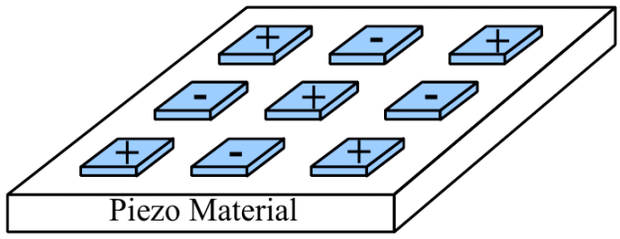

Figure 4. A 2D excitation structure based on a double potential alternation to promote the excitation of surface waves exhibiting complex polarization (the 2D equivalent of the usual interdigital transducer)

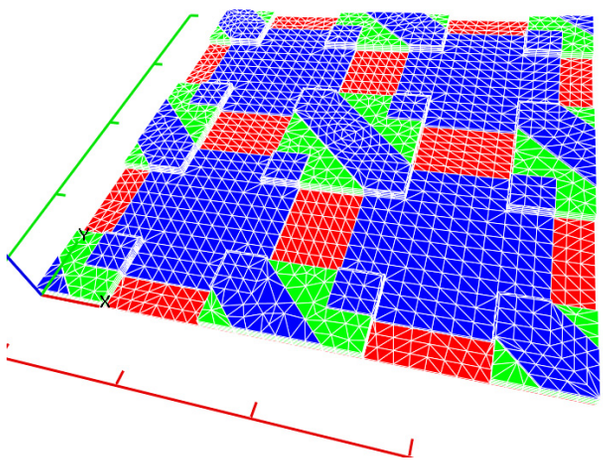

Figure 5. An example of simplified 3D mesh used to simulate the 2D periodic transducer. The period of the grating is set to 25Âţm. The green square dots localize the dielectric âĂŞ SiO2 âĂŞ spacers and the blue strips and squares show the deposition of the Al electrodes above the structure. The red background is the piezoelectric material.

used for the computation of the harmonic admittance of an infinite 2D periodic transducer according to the excitation conditions of figure 4. We then simply apply opposite potentials to the adjacent strips and set the two excitation parameters to an integer value (typically one). We particularly focused our interest on LiNbO3 and more specifically the (YXl)/128Âř cut because of its advantageous electromechanical coupling. The numerical and experimental results are drawn in figures 6. At a glance, the correspondence of the measured admittance with the harmonic conductance reported in is rather convincing about the fact that the device operates as theoretically announced. When focusing on the low frequency contributions, one can see that they are composed of two principal wide band contributions modulated by resonance peaks, expected to correspond to wave reflection on the surrounding devices in experimental measurements. Whatever the origin of this effect, this measurement proofs that the device actually can generate waves with clear electrical contribution on the device admittance and that quite sharp resonance can be expected, although the operation frequency remains rather low (near 100 MHz), corresponding rather fairly to theoretical predictions. To better understand the operation of the transducer, we have plotted the deformed shape of the surface for the two guided modes in figures 7. It turns out that the propagation takes place in both case along the median trace of the dielectric dots. In that case, the wavelength is then equal to 35.5μm, yielding the observed contributions near 100 MHz. In this configuration, the

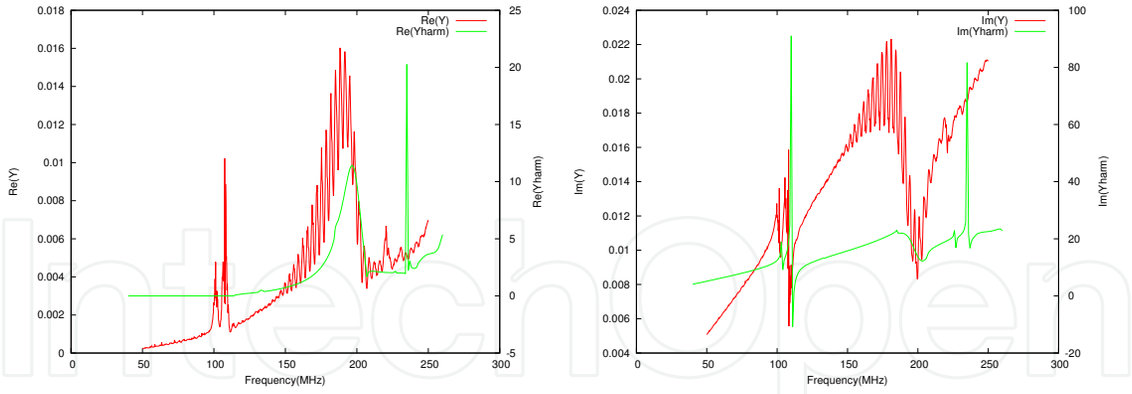

(a) Real part (b) Imaginary part

Figure 6. Harmonic admittance of the infinite 2D periodic grating of figure 5 focusing on the guided modes. In red experimental measurements and in green simulation.

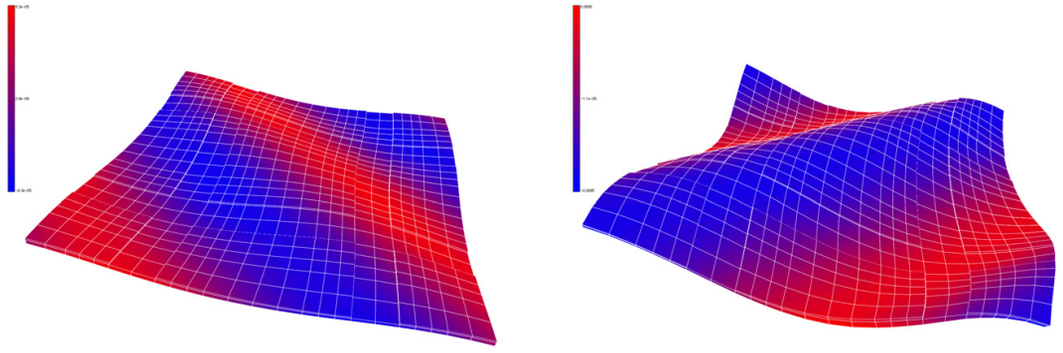

(a) Beginning of the stop-band (b) End of the stopband

Figure 7. Deformed mesh for both modes emphasized in figure 6 (isovalues correspond to displacement along x1)

transducer does not really allow for exciting complex propagation polarization but behaves more like a natural partially directionnal transducer (a small resonance at the beginning of the stop band but a large one at its end).

The improvements of experimental approaches lead to take into account new effects such as influence of SAW devices aperture. Indeed, up to now, the length of electrode is considered as infinite compare to the period of the grating in SAW resonators. So, the influence of the input buses and diffraction at the end of electrodes is neglected. However, this is a drastic assumption. Thus, to quantify such an influence, PML method is necessary to simulate the lateral leaky mode outside of the resonator. PML was already implemented in FEA [18, 19]. Nevertheless, a global approach to include PML in FEA is demonstrated below.

There are also more and more acoustic devices with finite lateral dimension such as BAW resonators or acoustic filter to avoid reflections at the end of SAW devices (Bragg mirrors). In some cases, it is possible to define a large periodicity in periodic FEA to model a non periodic structure and thus avoid the interaction between the neighbors (as in specific BAW resonators simulation). However, the computational time cost is very high. Moreover, in most cases, it is

not possible to use periodic FEA with high width. For example, the simulation of non periodic SAW resonators cannot be achieved in this way. So, the non-periodic FEA is necessary as well as the related boundary conditions i.e. the BEM [20].

Below, the main advancements of the FEA scheme applied to acoustic resonators with finite lateral dimension are depicted (such as dual mode filters or realistic periodic SAW resonators with effective aperture). The PML method as well as the BEM are thus demonstrated separately even if they are used together to simulate embedded finite resonator on radiating medium for instance.

3. FEA improvements

3.1. Boundary Element method in non-periodic cases

A radiating surface in an non periodic acoustic problem can be included to the FEA formalism in the right hand side of the general variational equation (1).

The right hand of equation (1) limited to the stress part stands for the radiation part. It can thus be treated by using Green's function based relation [21],

$$T_{ij}n_j = Gi_{ijk}(\omega, S)n_j * u_k, \tag{5}$$

where $*$ denotes the convolution between the displacements u and Gi, the inverse Green tensor relating the stress T to the displacement. Knowing the Green tensor, one can just insert equation (5) in equation (1) to solve the problem with radiation boundaries conditions without any restriction. We developed a first approach of this method for isotropic radiation medium in further work [8]. However, we can't apply straight this method for anisotropic medium. Indeed, the spectral Green function $\hat{Gi}(\omega, s)$ (where s is the slowness) is not holomorphe and so its inverse Fourier Transform (iFT) can't be computed directly for the general case (anisotropic medium). So to avoid this problem we use the reciprocal form of equation (5),

$$u_k = G_{ijk}(\omega, S) * T_{ij}n_j, \tag{6}$$

in which the direct green function G relates the displacements to the stress [21]. This function is defined from its iFT in the slowness space,

$$G_{ijk}(\omega, x_1) = \frac{\omega}{2\pi}\int_{-\infty}^{+\infty} \hat{G}_{ijk}(\omega, s_1)\exp(j\omega s_1 x_1)ds_1, \tag{7}$$

where $\hat{}$ defines the Fourier Transform. s_1 is the slowness along the direction x_1. To avoid the problem of loading or time calculation, we use the canonical Green function $\hat{H}(s_1)$ [22] which is frequency independent. This function is related to the Green function as following

$$\hat{G}_{ijk}(\omega, s_1) = \frac{\hat{H}_{ijk}(s_1)}{\omega}. \tag{8}$$

Thus we are able to compute the canonical function before the FEA once and for all assuming the radiation medium is semi-infinite [23]. The actual Green function is obtained by including the equation (8) in equation (7),

$$G_{i2k}(\omega, x_1) = \frac{1}{2\pi}\int_{-\infty}^{+\infty} \hat{H}_{i2k}(s_1)\exp(j\omega s_1 x_1)ds_1. \tag{9}$$

(Here the notation takes into account the propagation and radiation assumptions of this work i.e., $j = 2$). However, the spectral canonical Green function $\hat{H}(s_1)$ gives rise to some singularities. So, we must to divide up this function into three parts [24]

$$\hat{H}_{i2k}(s_1) = \hat{H}_{i2k}^{(res)}(s_1) + \hat{H}_{i2k}^{\infty}(s_1) + \hat{H}_{i2k}^{(0)}(s_1) + \hat{H}_{i2k}^{R}, \tag{10}$$

where $\hat{H}_{i2k}^{(0)}(s_1)$ is the contribution for the slowness $s_1 = 0$, $\hat{H}_{i2k}^{\infty}(s_1)$ is the asymptotic one and $\hat{H}_{i2k}^{R}$ stands for the acoustic poles contribution. Thus, we can define $\hat{H}_{i2k}^{(res)}(s_1)$ as the residual Green function part without singularities. The computation in the spectral domain as well as in the spatial one always takes into account separately these four parts. The residual part can be numerically computed whereas the others need to be considered analytically [24].

Once, the Green function numerically and/or analytically defined, one can express the variational form of equation (6),

$$\begin{aligned} &\int_{x_1=-\infty}^{x_1=+\infty} \delta u_k^* u_k(x_1) dx_1 = \\ &\int_{x_1=-\infty}^{x_1=+\infty} \delta u_i^* \int_{x_1'=-\infty}^{x_1'=+\infty} G_{i2k}(\omega, x_1 - x_1') T_{i2}(x_1') dx_1' dx_1, \end{aligned} \tag{11}$$

in order to develop the Finite Element scheme for the radiation conditions,

$$\begin{aligned} &\sum_{e=1}^{N_e} \sum_{m=1}^{\eta_e} \delta {u_k}^{*(em)} \sum_{\mu=1}^{\eta_e} u_k^{(e\mu)} \int_{\Gamma_e} P^{(em)}(x_1^e) P^{(e\mu)}(x_1^e) dx_1 = \\ &\sum_{e=1}^{N_e} \sum_{m=1}^{\eta_e} \delta {u_k}^{*(em)} \sum_{\epsilon=1}^{N_e} \sum_{\mu=1}^{\eta_e} T_{i2}^{(\epsilon\mu)} \int_{\Gamma_e} P^{(em)}(x_1^e) \\ &\int_{\Gamma_\epsilon} P^{(\epsilon\mu)}(x_1^\epsilon) G_{i2k}(\omega, (x_1^e - x_1^\epsilon)) dx_1^\epsilon dx_1^e, \end{aligned} \tag{12}$$

where N_e is the number of elements on Γ_2 and η_e the number of nodes by element. $P^{(em)}$ are the FEA interpolation polynomials (first or second degree). The integrations from $-\infty$ to $+\infty$ are bound to the Γ_2 length. Indeed, anywhere else that the activated domain the Green function is null. Note also that the nodal displacement, variational unknown and stress are outside the convolution and the integrals on the elements.

So to match the FEA algorithm, we must write equation (12) in a nodal matrix relation,

$$< \delta u > (\Psi) \{u\} =< \delta u > (G) \{T\}, \tag{13}$$

where (Ψ) is the nodal matrix relating the nodal vectors of the variational unknown and displacements. In the same way, (G) is the nodal Green matrix relating the nodal vectors of the variational unknown and stress. Equation (13) is right whatever the variational unknown. So, on can write the reciprocal relation relating the stress to the displacement,

$$\{T\} = (G)^{-1}(\Psi) \{u\}, \tag{14}$$

where $(G)^{-1}$ is the inverse of the nodal Green matrix defined in equation (12,13). The general variational equation (1) must be also written in a matrix formulation (Only the elastic part is considered without losses of generality)

$$< \delta u > \left[K - M\omega^2\right] \{u\} =< \delta u > (\Psi) \{T\} . \tag{15}$$

Thus the final FEA/BEM system is obtained by including equation (14) in equation (15),

$$\left[K - M\omega^2 - (\Psi)(G)^{-1}(\Psi)\right] \{u\} = 0. \tag{16}$$

the global FEA/BEM system is similar to the ideal case with an additional correction which doesn't change the scheme to solve the problem.

3.2. Perfectly Matched Layer method

The PML method was first developped in electromagnetism [25] and well adapted to the Finite Difference in Time Domain (FDTD) method [26]. More recently, some works demonstrated the implementation of this approach for acoustic simulations based on FEA [18] [19]. The basic idea consists in rigorously simulating an exponential decrease of the acoustic field along at least one space direction. To clear the approach, let us consider the following incident plane wave

$$u = Aexp^{-j(k_x x - \omega)} = Aexp^{-j\omega(s_x x - t)} \tag{17}$$

We then consider that in the absorbing area, one can apply a geometrical transform in the complex plane to introduce the exponential decay. Since it must not modify the propagation phase, this transform can be written

$$\tilde{x} = x - jf(x) \tag{18}$$

where $f(x)$ growths from the origin of the absorbing area to its end along a defined rate. However, since this transform must be efficient for any frequency (we represent the problem in the spectral domain), it is wise to define this function as follow :

$$f(x_i) = \frac{1}{\omega} \int_0^{x_i} d(x) \mathrm{dx}, \tag{19}$$

$$d(x_i) = d_{max} \left(1 - \frac{(abs(x_i) - x_p)^2}{(x_a - x_p)^2}\right)^n, \tag{20}$$

which allows for an easy definition of the transform Jacobian linking the considered coordinate systems. This reads

$$\frac{1}{\partial \tilde{x}} = \frac{j\omega}{j\omega + d(x)} \frac{1}{\partial x} \rightarrow \frac{1}{\partial x} = \left(1 + \frac{d(x)}{j\omega}\right) \frac{1}{\partial \tilde{x}} = \alpha_x \frac{1}{\partial \tilde{x}} \tag{21}$$

Replacing x by $\tilde{x}$ in (17) provides the wanted exponential decay if $f(x)$ unconditionally growths, imposing $d(x)$ even and positive to fulfil the absorbing condition for any x (we assume the problem centred around $x = 0$). Since the absorbing function $d(x)$ is not frequency dependent, its efficiency should be constant along ω. Conformably to Zheng and Huang [27],

we develop a formulation based on the usual piezoelectricity equations, yielding significant modifications of the elastic, piezoelectric and dielectric constants to account for the absorption.

We now rewrite the elasticity equations in the absorbing region turning x to $\tilde{x}$, using then (5) to express the result in the initial coordinates. As in [27], the absorbing effect is assumed along the three space directions for the sake of generality. The equilibrium equation then reads

$$-\rho\omega^2 u_i = \frac{\partial T_{ij}}{\partial \tilde{x}_j} = \frac{1}{\alpha_j}\frac{\partial T_{ij}}{\partial x_j} \tag{22}$$

where α_j is characterized by its specific function $d_j(x_j)$. T_{ij} and u_i respectively represent the dynamic stresses and displacements, and ϱ is the mass density. We introduce a non symmetrical stress tensor, expressed in the transformed axis

$$\tilde{T}_{ij} = \frac{\alpha_1\alpha_2\alpha_3}{\alpha_j} C_{ijkl}\frac{\partial u_l}{\partial \tilde{x}_k} = \frac{\alpha_1\alpha_2\alpha_3}{\alpha_j\alpha_k} C_{ijkl}\frac{\partial u_l}{\partial x_k} = \tilde{C}_{ijkl}\frac{\partial u_l}{\partial x_k} \tag{23}$$

where $\tilde{C}_{ijkl}$ is the transformed elastic constant tensor relative to the absorption area. We multiply (22) by $\alpha_1\alpha_2\alpha_3$, thus yielding Newton relation for PMLs in the real coordinates

$$-\tilde{\rho}\omega^2 u_i = \frac{\partial \tilde{T}_{ij}}{\partial x_j} \tag{24}$$

where $\tilde{\rho} = \rho\alpha_1\alpha_2\alpha_3$ is the mass density relative to the transformed domain. Since the obtained form of the equilibrium equation complies with the classical expression for usual solids, it is liable to exploit the standard FEA formulation for PML as well, accounting for the frequency dependence of the transformed physical tensors. These developments of course can be extended to piezoelectricity by rewriting Poisson's equation and taking into account the piezoelectric coupling in the stress definition as follows

$$\begin{gathered}\tilde{T}_{ij} = \frac{\alpha_1\alpha_2\alpha_3}{\alpha_j}\left(C_{ijkl}\frac{\partial u_l}{\partial \tilde{x}_k} + e_{kij}\frac{\partial \varphi}{\partial \tilde{x}_k}\right) = \\ C_{ijkl}\frac{\partial u_l}{\partial x_k} + \tilde{e}_{kij}\frac{\partial \varphi}{\partial x_k}\end{gathered} \tag{25}$$

Poisson's equation expressed in the transformed system of axes reads

$$\frac{\partial D_i}{\partial \tilde{x}_i} = 0 \Rightarrow \frac{1}{\alpha_i}\frac{\partial D_i}{\partial x_i} = 0 \tag{26}$$

with D_i the electrical displacement vector. To provide an homogeneous formulation, we proceed as for the stress definition (23), multiplying the electrical displacement by $\alpha_1\alpha_2\alpha_3$, yielding

$$\tilde{D}_i = \frac{\alpha_1\alpha_2\alpha_3}{\alpha_i} D_i \tag{27}$$

As for the propagation equation (22), the Poisson's condition is written accounting for these changes as

$$\frac{\partial \tilde{D}_i}{\partial x_i} = 0 \tag{28}$$

Conformably to the stress tensor transformation, we introduce modified piezoelectric and dielectric constants defined as follows

$$\tilde{D}_i = \frac{\alpha_1\alpha_2\alpha_3}{\alpha_i}\left(e_{ikl}\frac{\partial u_l}{\partial \tilde{x}_k} - \varepsilon_{ik}\frac{\partial \varphi}{\partial \tilde{x}_k}\right) = \tilde{e}_{ikl}\frac{\partial u_l}{\partial x_k} - \tilde{\varepsilon}_{ik}\frac{\partial \varphi}{\partial x_k} \tag{29}$$

We now are able to establish a FEA formulation exploiting these developments without fundamental changes of the existing code. Thus, equation (1) becomes

$$\begin{aligned}\iiint_{\Omega_{PML}}\left(\frac{\partial \delta u_i}{\partial x_j}\tilde{C}_{ijkl}\frac{\partial u_l}{\partial x_k} + \frac{\partial \delta u_i}{\partial x_j}\tilde{e}_{kij}\frac{\partial \phi}{\partial x_k} + \frac{\partial \delta \phi}{\partial x_i}\tilde{e}_{ijk}\frac{\partial u_j}{\partial x_k}\right.\\ \left. - \frac{\partial \delta \phi}{\partial x_j}\tilde{\varepsilon}_{jk}\frac{\partial \phi}{\partial x_k} - \rho\omega^2 u_i \delta u_i\right) dV =\\ \iint_{\Gamma_{PML}}\left(\delta u_i \tilde{T}_{ij} n_j + \delta\phi \tilde{D}_j n_j\right) dS\end{aligned} \tag{30}$$

where Ω_{PML} and Γ_{PML} are respectively the PML domain and its boundary.

We must note here that all the parameters of the absorbing polynomial (Eqs. (19) and (20)) are empirically defined. Indeed, the polynomial $d(x)$ must increase from zero to the maximum value $dmax$ by a progressive slope. The value of $d(x)$ must be zero at the beginning of the PML to verify the impedance match. Moreover, the derivative of $d(x)$ must be null too to avoid any singularities. However, the absorbing polynomial must increase as quick as possible to minimize the number of PML finite elements with respect to the better smoothy shape. Therefore one can choose the degree of polynomial $d(x)$ equal to 3. The depth of the PML domain $(x_p - x_a)$ is also defined according the absorbed waves. So, we defined that this length must be approximately equal to one wavelength.

4. Results

In this section, we first depict results from the Boundary Element Method based on the direct Green function. Next, the 2D and 3D results of the Perfectly Matched Layer method are exhibited. At last, we depict how powerful the mixed approached is on a 2D case.

4.1. A Green's function as boundary condition

4.1.1. Validation by comparison with proofed periodic FEA scheme

First, the non periodic numerical scheme developed here is compared to an existing periodic one that we developed in previous works [15]. In order to make this comparison, we choose the configuration depicted in figure 8. It seems to be odd to test a non periodic code with a periodic one. However, in the configuration of figure 8, the most of waves provided by the transducer propagate into the direction x_2. Of course, there are some components along the x_1 due to the coupling with the radiation surface or the finite width of the transducer. So, we choose a period $p = 1.2$mm which makes insignificant the coupling with nearest neighbor in the periodic case at Γ_3. This choice also allows us to neglect the reflections at the en of the mesh for the non periodic case on Γ_3. The results of the periodic computation have been

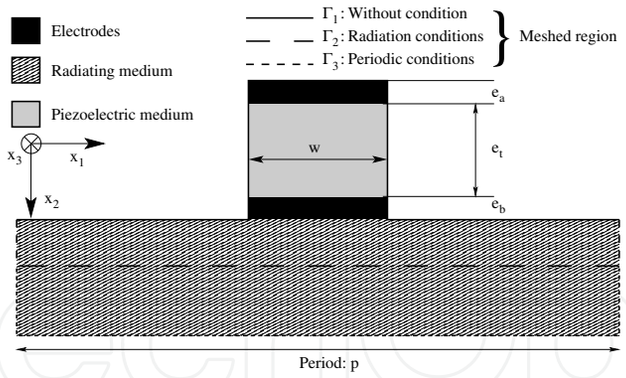

Figure 8. Chosen geometry for the validation by comparison with periodic FEA code. This configuration defines a single transducer providing mainly bulk wave.

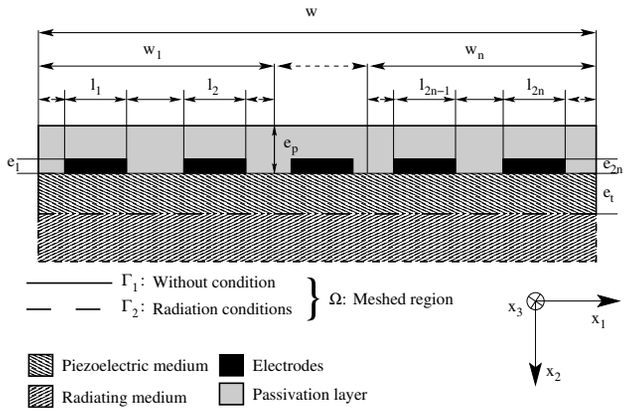

Figure 9. General geometry of resonator studied addressed by the investigated FEA-BEM. This configuration defines a non periodic interdigital transducers grating devoted to SAW applications

tested to be unchanged from the chosen period $p = 1.2$mm. The thickness of electrodes is set to zero and so we don't consider the influence of the mass loading and material. However, it's not a restriction due to the numerical method and a study of the influence of the electrode material could be achieved. The width of the piezoelectric transducer is set to $w = 100\mu$m, its thickness is $e_t = 4\mu$m. we also choose the same material for the radiation medium and the piezoelectric one. The constants used for computation are these of quartz with a YXl/36 cut. The surrounding medium is the vacuum. In figure 10, we show this comparison between the periodic and the non periodic code. In this computation, we consider all the degrees of freedom i.e., all modes can be observed (the in plane one as well as the shear one). The figure 10(a) depicts the conductance whereas figure 10(b) draws the susceptance both computed for the above configuration. The good agreement between these two different methods is the first proof of validation for the non periodic scheme presented in this work.

4.1.2. Validation by comparison with an other non periodic scheme

The second test presented here is the comparison with a non periodic method based on the integral equations method [24]. The configuration is the one depicted in figure 9. It addresses a SAW devices of finite width equal to $w = \sum_{i=1}^{n} w_i$. w_i is the width of the pattern and n is the number of electrodes pairs. The pattern k is defined by a pair of metallic electrodes. The widths and the thicknesses of each electrodes for the considered pattern are respectively denoted by l_{2n-1}, e_{2n-1} and l_{2k}, e_{2n}. The metal ratio is constant and set to 0.5. The width of the

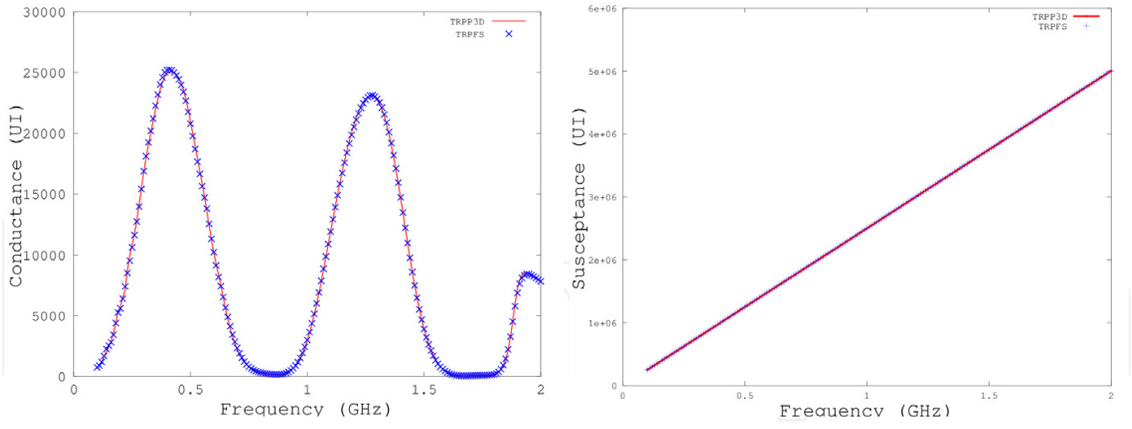

(a) Conductance (μS) (b) Susceptance (μS)

Figure 10. Comparison between the results obtained with a proofed periodic computation (TRPP3D) and the method presented in this work (TRPFS). All the degrees of freedom are taken into account and the FEA interpolation is quadratic. All elements of the mesh are identical (triangle, 2 elements per micron in x_1 and 10 elements in x_2).

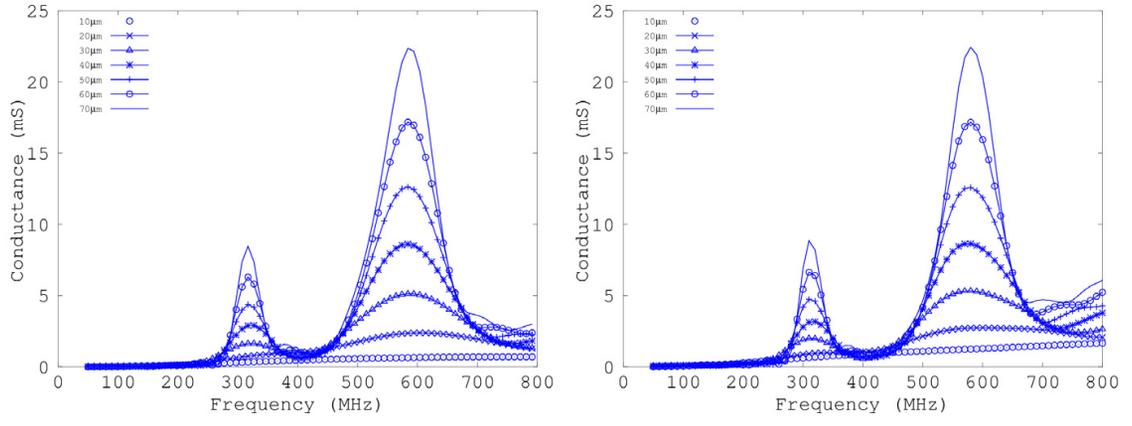

(a) Integral equations method (b) FEA/BEM

Figure 11. Comparison between the results obtained with an integral equations based method and the FEA/BEM method presented in this paper. All the degrees of freedom are taken into account and the FEA interpolation is quadratic. The mesh is the same as previously.

piezoelectric medium is w and its thickness is $e_t = 200nm$. The piezoelectric material constants used for computation are still these of quartz with a YXl/36 cut. The radiation medium is also the same as the previous test with periodic method. As previously, the surrounding medium is still the vacuum. Here, all the electrodes widths are equal to 2.5μm and they are without thickness i.e., there is no mass loading. So the total width of the SAW device is $w = 10n\mu$m. We increase the number of pairs of electrodes from 1 to 7. Thus, w varies from 10μm to 70μm. The excitation is the excitation is an symmetric alternate potential for each pattern i.e. $+U/-U$ where $U = 0.5V$.

The results of this comparison are drawn in figure 11. The figure 11(a) depicts the results for the integral equations method. Those of the FEA/BEM methods are in figure 11(b). Once

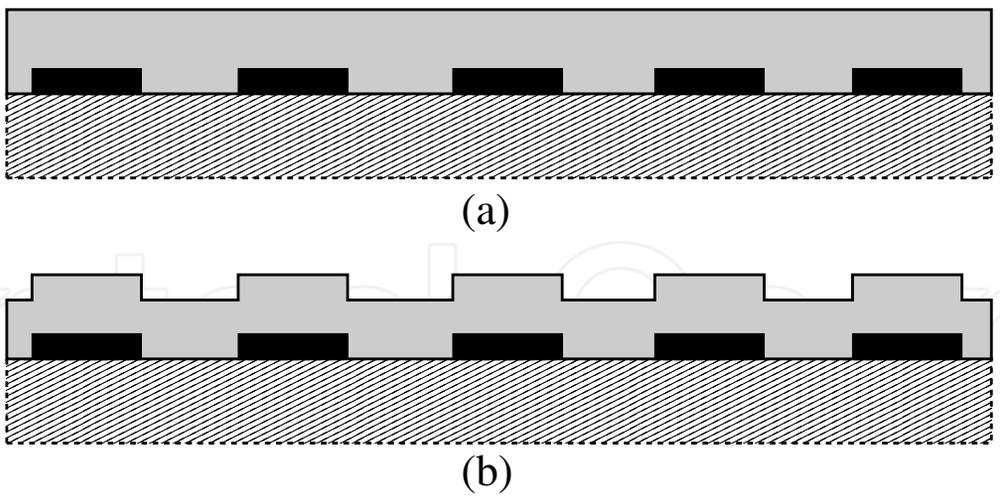

Figure 12. Geometrical configuration for a passivated electrodes grating with (a) non conformal and (b) conformal deposition. The electrodes thickness is either null or equal to 200nm. The other parameter still unchanged with the configuration depicted in figure 9.

again, the good agreement between the two method allows us to conclude that the FEA/BEM method is a good tools for the understanding the behavior of such a SAW devices.

4.2. Application to a wide non periodic passivated SAW devices

The method presented in this work is devoted to address non periodic passivated SAW devices among others. So, we give here some results about this configuration. We consider the same configuration as in the case depicted in figure 9. We only vary the thickness of electrodes. First we let them without thickness and look at the influence of the passivation layer and next we consider a electrodes thickness equal to 200nm. We then study again the device behavior against the passivation configuration i.e., without passivation, with conformal passivation and with non conformal passivation (See figure 12). The material constants of the passivation layer are to be the fused silicon ones. These results are depicted in figure 13. We can see that the global effect of then passivation layer red-shift the resonance frequencies for the non massive electrodes as well as for the massive one. Indeed, this layer acts as a mass loading effect. So, the resonance frequency must decreases with the mass over the electrodes. Moreover, this conclusion is corroborated by the evolution between the cyan and magenta curves of figure 13. The frequency is slightly lower for the conformal passivation which leads to a higher weight over electrodes. We also point out that the conductance level increases when we put the passivation layer. This comment can be explained by considering the velocity of the mode in the passivation layer is higher than in the guide. So the guidance is better for the case with passivation layer. These results are in good agreement with previous results obtained on periodic structures [15].

4.3. Perfectly Matched Layer Method: an other approach

The efficiency of the PML implemented in FEA is depicted in three parts. First, a 2D-case is investigated showing the absorbing due to the PML domain and the effects of the effects of the finite lateral size on the behavior of a SAW resonator. Next, the same study is repeated but in a 3D configuration in order to validate the general PML approach. At last, a realistic SAW

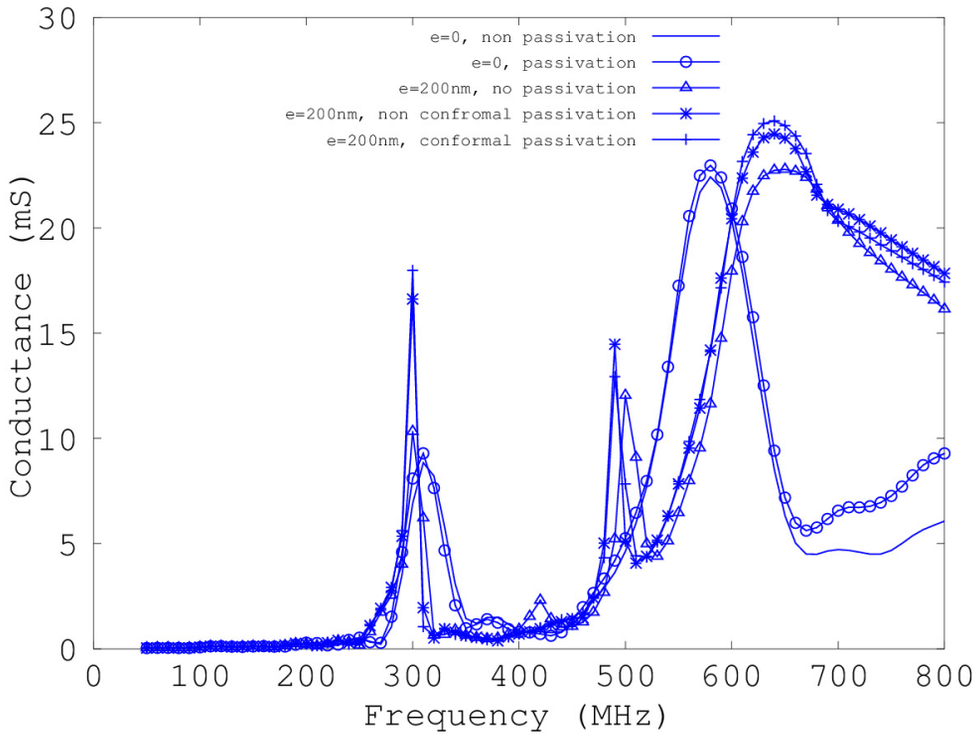

Figure 13. Conductance in (mS). Influence of the passivation layer on the acoustic device behavior (figure 9). All the degrees of freedom are taken into account and the FEA interpolation is quadratic. The same FEA mesh is used.

problem is addressed by considering the aperture of the resonator and absorbing the lateral leaky modes.

First, A 2D SAW resonator problem is addressed. The geometrical configuration is depicted in figure 14. A piezoelectric medium (quartz YXl/36) is driven by 4 pairs of electrodes. The electrodes are non massive and alternatively activated with $V = 1V$ and $V = 0V$. The period is $10\mu m$. The depth of PML on both sides is $35\mu m$. The eight of the mesh is $75\mu m$. The absorbing parameters are set to $dmax = 10^6$ and $n = 3$. The result of this simulation is shown in figure 15. We depicted the vibrations for the x-displacements in the XY plane. The vibrations in both the right and left PML domains are strongly reduced as and as they enter into. The decreasing factor is around 10^{-5}. We also hardly observed the phenomena of diffraction due to the finite lateral size of the resonator. Indeed, weak lobes appears at the both lateral end of the grating and give rise to bulk wave and so losses in the medium.

Next, we repeat the same simulation as the one depicted in figure 14 but for a 3D geometry. The configuration is drawn in figure 16. The piezoelectric is once more quartz YXl/36. The same set of non massive electrodes is still powered in the same way. The absorbing conditions are also the same.

The x-displacement obtained by FEA/PML is shown in the perspective figure 17. It is clearly demonstrated that the vibration have the same absorption as in the 2D-case even if the absorbing factor is slightly worse. One more time, the losses in the medium can also be observed at the end of the resonator. We notice that there is no relection at the end of the mesh for both side edges and bottom boundaries.

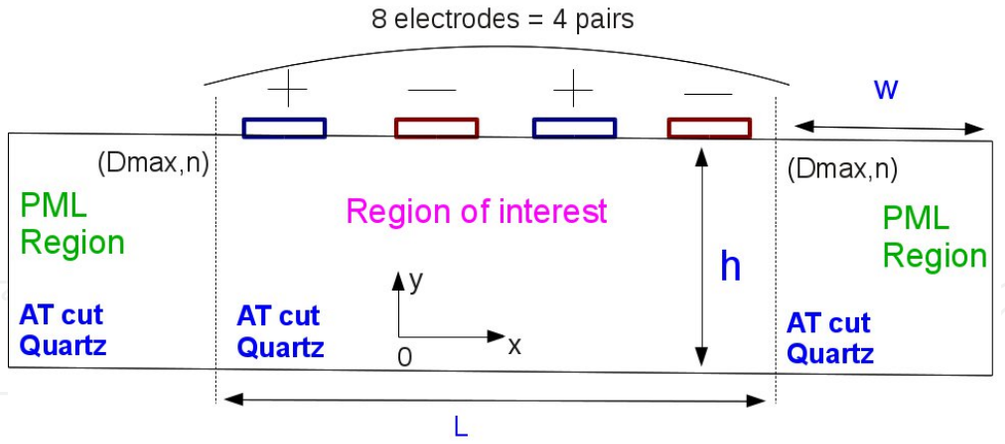

Figure 14. Characteristic configuration for finite SAW resonators considering the mixed PML/FEA approach. Eight non massive electrodes are activated alternatively ($V_1 = 1V$, $V_2 = 0V$). The width of electrodes is equal to $2.5\mu m$ and the period of the resonator is set to $10\mu m$. The piezoelectric medium is quartz YXl/36. Its thickness vary from zero. On the left and right parts of the scheme, two PML domains are set. No boundary conditions are defined neither at the top nor at the bottom. Th depth of the piezoelectric h is chosen to avoid any interaction with the penetrating bulk wave at the bottom interface. $dmax = 10^6$ and $n = 3$.

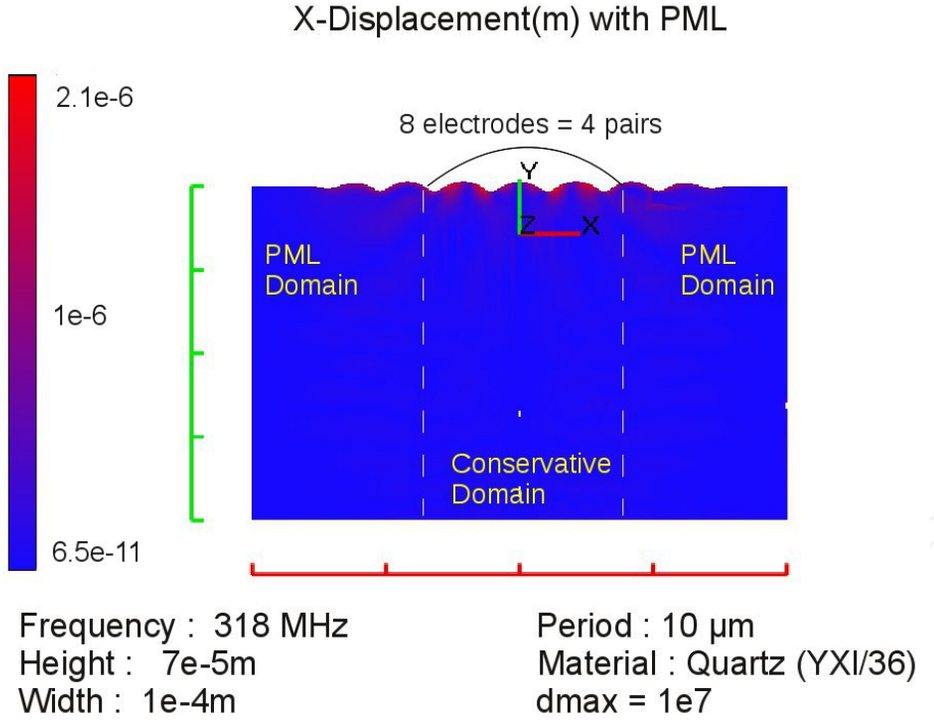

Figure 15. The vibrations for x-displacement in the XY plane for the 2-D problem depicted in figure 14. The piezoelectric medium is quartz YXl/36 activated by eight electrodes alternatively powered by $V = 1V$ and $V = 0V$. The PML domains are delimited by the white dashed line at the let and right sides. The frequency is $318MHz$. $h = 7e-5m$, $dmax = 10^6$ and $n = 3$.

The last configuration highlight a new point to design SAW resonator. Indeed, up to now, the devices modelings were most often considered as 2D systems infinitely periodic in the direction of propagation and infinite in the perpendicular one. We just demonstrate that it

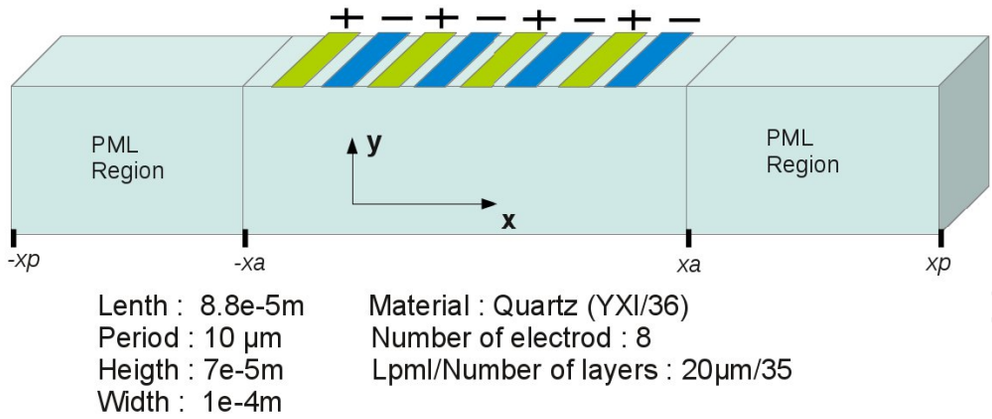

Figure 16. Same configuration as in figure 14 but in 3D-case. The z-direction is periodically infinite. So the electrodes are infinitly long in the z-direction. Eight non massive electrodes are activated alternatively ($V_1 = 1V$, $V_2 = 0V$).$h = 7e-5m$, $dmax = 10^6$ and $n = 3$.

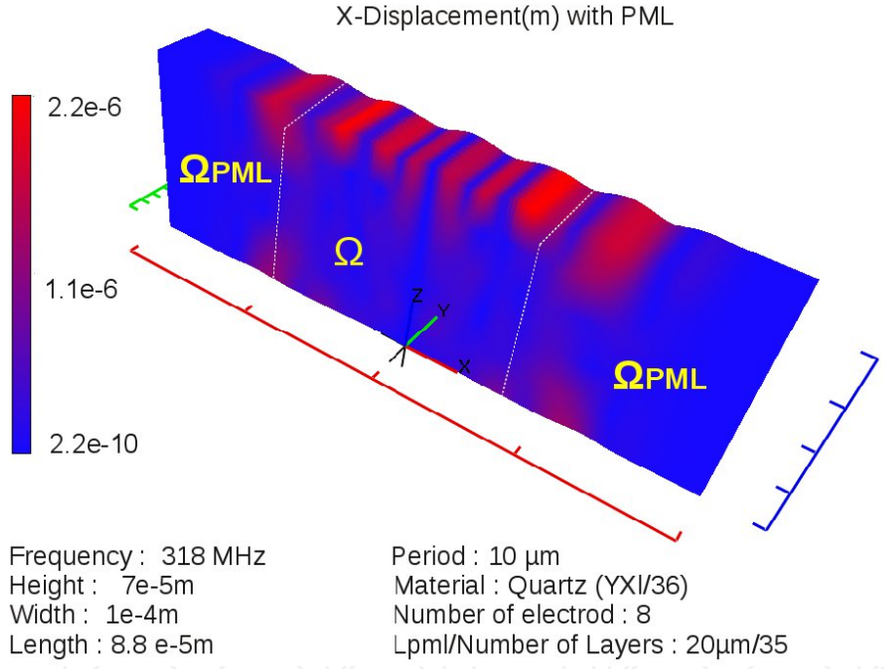

Figure 17. The vibrations for x-displacement for the 3-D problem depicted in figure 16. The piezoelectric medium is quartz YXl/36 activated by eight electrodes alternatively excited by $V = 1V$ and $V = 0V$. The PML domains are delimited by the white dashed line at the let and right sides. The frequency is $318MHz$. $h = 7e-5m$, $dmax = 10^6$ and $n = 3$.

is now possible to take into account the effects due to finite dimension along the direction of propagation. In this part, we depict the way to address the problem of real aperture of a SAW resonator. In other words, we consider a finite dimension in the perpendicular direction of the propagation. In this study, the number of electrodes is infinite. The geometrical configuration is depicted in figure 18. The materials properties, excitation and dimensions of the grating are still the same as previously in figure 16. We now consider a length of the electrodes equal to $54\mu m$ for a period in the direction of propagation equal to $10\mu m$. The buses on the both right and left gratings are infinite along the propagation and $20\mu m$ wide. We also assume that the

piezoelectric medium continue towards the infinity on the both sides of the resonator. The PML method allows this assumption.

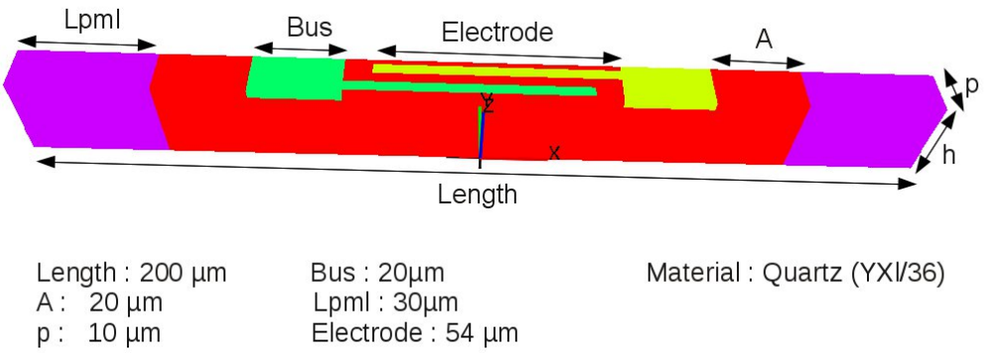

Figure 18. Configuration of an infinitely periodic SAW resonator in the propagation direction but with finite lateral dimension. The z-direction is infinitely periodic and the non massive electrodes are alternatively excited with $V_1 = 1V$ and $V_2 = 0V$. The piezoelectric medium is quartz YXl/36. The length of electrodes is $54\mu m$ while the period is $10\mu m$. $h = 30\mu m$, $dmax = 1e-6$ and $n = 3$.

Once again, we show the vibration for the x-displacement in the perspective figure 19. The factor of absorption is still very high even if we notice a slight decrease. The Ω domain stands for the physical space in which the SAW is generated. We observe the Rayleigh wave in the middle of Ω. On each side of this vibration, the presence of th buses is denoted by two maxima of displacement. This displacements give rise to a lateral mode which is reflected on the side edges if there is no activated PML. But, in figure 19, all PML are turned on. So, the lateral modes can be detected at the very end of the Ω area, just before the PML domains. However, due to the presence of the PML, this mode do not reflect on the side edges and moreover its amplitude decreases at the time it progress in the PML from the beginning to the end where it almost vanishes by then.

These three results show the efficiency of the combining of PML and FEA to simulate the effects due to the consideration of the real length or width of a SAW resonator. Thus, using this kind of method, we are able to simulate realistic effects in SAW. This method can also be applied to other kind of resonator.

4.4. The mixed BEM/PML approach

In the last part of the results exhibiting, the complete mixed BEM/PML approach is highlighted. This is done considering the general SAW configuration in figure 9 and adding PML area. This configuration is depicted in figure 20. A finite SAW resonator is characterized considering both the PML and the BEM as boundary conditions. The piezoelectric medium is a YXl/36 quartz. Its thickness can increase from zero to a non null value. It's excited by two non massive electrodes. The width of each electrodes is equal to $2.5\mu m$ and the length of the resonator is $10\mu m$. The excitation is symmetric and $V_1 = -V_2 = 0.5V$. The number of finite elements by length unit is equal to $1.6e6$ $elements/m$ along x direction and $6e5$ $elements/m$ along y. The PML domains have the same FEA properties except for the absorbing conditions. The absorbing coefficient $dmax$ is equal to $1e-6$ and the order of the polynomial is set to $n = 3$. The BEM stands for the bottom radiation on Γ_β and simulates the propagation to the infinite in the same medium as the piezoelectric one. It's important to note

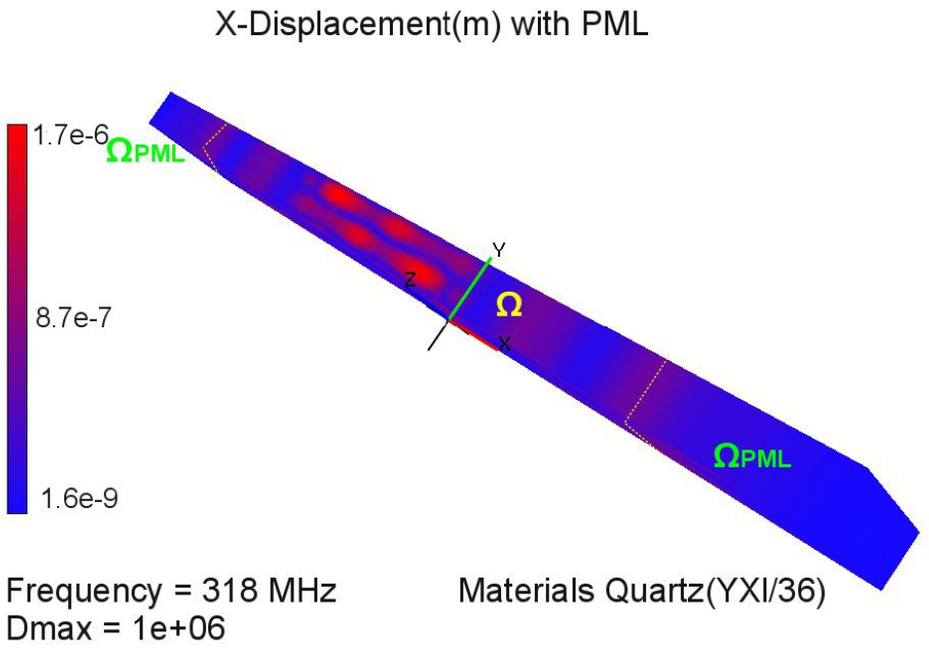

Figure 19. The vibrations for x-displacement for the 3-D problem depicted in figure 18. The piezoelectric medium is quartz YXl/36 activated by eight electrodes alternatively excited by $V = 1V$ and $V = 0V$. The PML domains are delimited by the white dashed line at the let and right sides. The frequency is $318MHz$. $h = 7e-5m$, $dmax = 10^6$ and $n = 3$.

that the BEM introduces an infinite slab in the x direction under the piezoelectric medium. So if the thickness of the piezoelectric is zero, the two electrodes are placed on an infinite layer of YXl/36 quartz.

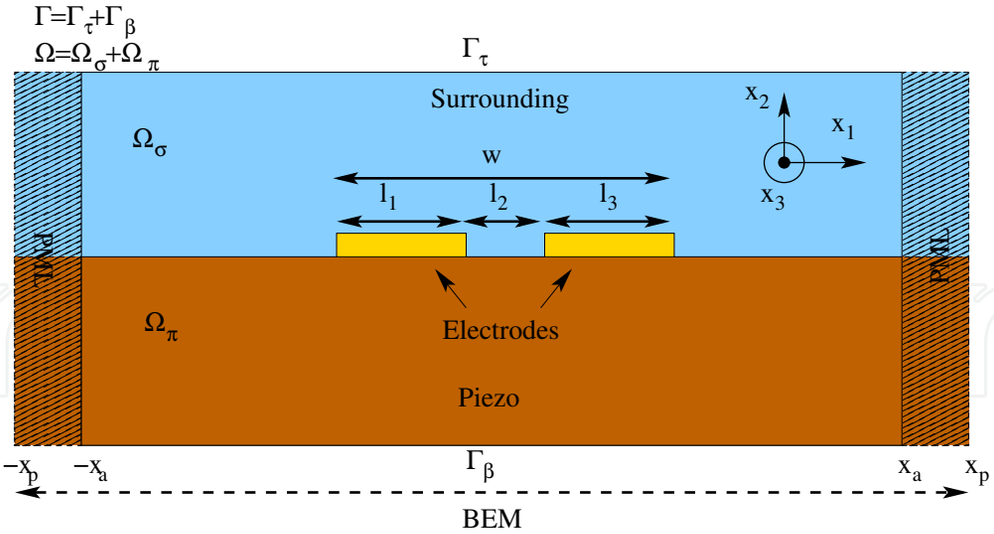

Figure 20. Characteristic configuration for finite SAW resonators considering the mixed BEM/PML approach. Two non massive electrodes are activated ($V_1 = 0.5V$, $V_2 = -0.5V$). The width of electrodes is equal to $2.5\mu m$ and the period of the resonator is set to $10\mu m$. The piezoelectric medium is quartz YXl/36. Its thickness vary from zero. Only the radiation on Γ_β is active and the radiating medium is the same as the piezoelectric one. The surrounding medium is vacuum so there is no radiation on Γ_α. On the left and right parts of the scheme, two PML domain are added.

We first focused on the effects of the thickness of the piezoelectric medium on the response of the resonator to an electric excitation. The excitation and the geometric configuration are depicted in figure 20. This response is exhibited in figure 21. We depict the logarithm of the conductance expressed in micro Siemens against the frequency for different thicknesses of the piezoelectric medium. The depth of the piezoelectric medium increases from zero for the red solid line to 2 microns for the red stars. It can be noted that when the thickness decreases the conductance converges to the result of the infinite slab, i.e. when the thickness is zero. This evolution can be explained by the diffraction at the end of the resonator when the depth is non zero. So even is the behavior is nearly the same whatever the thickness of the piezoelectric, the influence of this parameter is actually important.

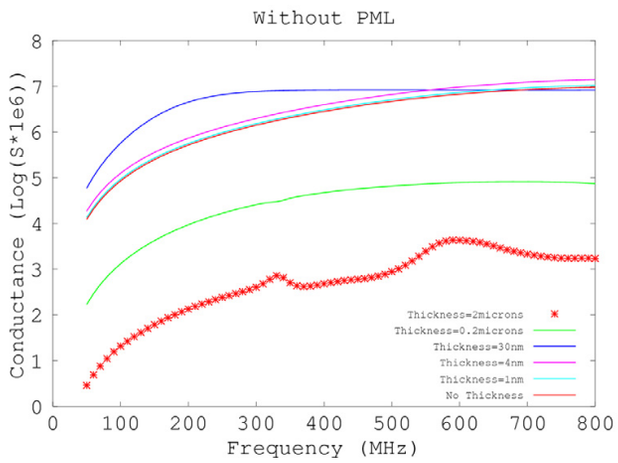

Figure 21. The logarithm of the conductance in μS against the frequency for different thicknesses of the piezoelectric medium when the PML is switch off. The radiation in the substrate is simulated with BEM. The width of the transducer is finite and equal to $10\mu m$ and the PML domains vanish. The electrodes are non massive. The number of finite elements by length unit is equal to $1.6e6\ elements/m$ along x direction and $6e5\ elements/m$ along y.

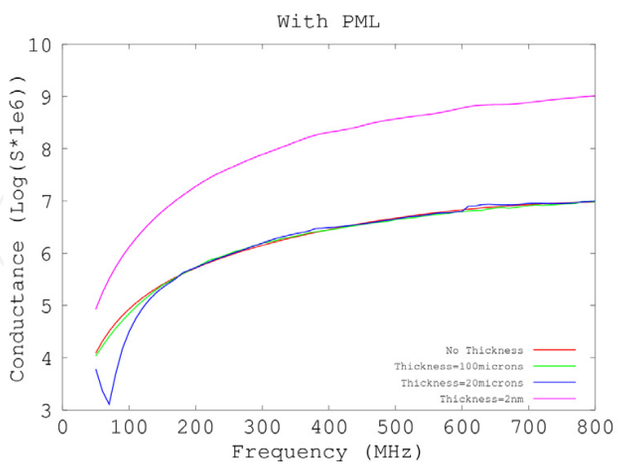

Figure 22. The logarithm of the conductance in μS against the frequency for different thickness of the piezoelectric medium when the PML is switch on. Except for PML domains, the configuration is the same as in the figure 21. The width of PML Domains is equal to $30\mu m$ for the both right and the left part. The number of finite elements by length unit is the same as outside PML domains. The absorbing coefficient is set to $dmax = 1e6$ and the polynomial order is equal to $n = 3$.

So to highlight the PML efficiency, we compare the results of the thickness equal to zero in figure 21 to the non-zero ones when the PML are activated. The same configuration as in figure 21 is used for the non PML area, we only add two PML on the right and the left parts. The depth of the PML domains is equal to $x_p - x_a = 3\mu m$. The absorbing coefficients are defined above. Again, the variation of the conductance against the frequency is depicted for different thickness of piezoelectric when PML is switch on in figure 22. We can notice again that the conductance converges to the result for a zero thickness when the piezoelectric depth increases. That means there is a non zero interaction between PML and BEM giving rise to undesirable effects for low thickness. So, It's again important to notice that the mixed of the two boundary conditions PML and BEM must be used in a drastic validity domain. One must consider a sufficient thickness of piezoelectric medium or used a zero thickness without PML. The last way can be used if no surrounding medium is taken into account. However, in the configuration of figures 12, the PML must be used for an infinite passivation layer and we must check if the simulation is in the validity domain.

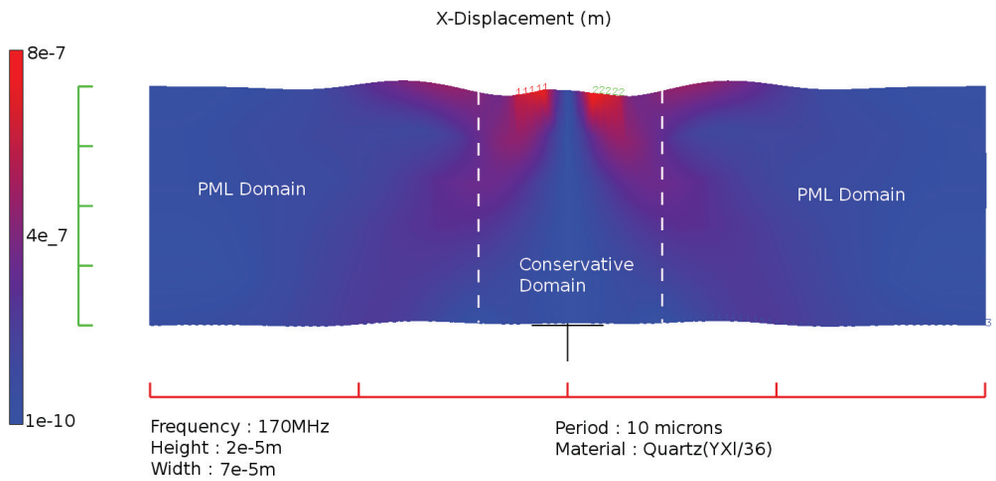

Figure 23. The map of x-displacement in the XY plane for the fixed frequency $170MHz$. The configuration is the one depicted in figure 20. The height of the piezoelectric medium is set to $2e5m$. The electrodes are denoted by the references 1 and 2. The PML domain are delimited by the white dashed line. The BEM is set at the bottom of the meshed domain also in PML area.

The last part of the results on mixed PML/BEM approach shows the effects of the boundary conditions on the x-displacement in the sagittal plane (XY). The distortion is depicted in figure 23. This is due to the electric excitation of the piezoelectric medium located in references 1 and 2. This result is obtained for a fixed frequency equal to 170MHz for the previous geometrical configuration of figure 22 for a $20\mu m$ thickness. The PML areas are denoted by the white dashed line and the conservative part (or the physical one) is under the electrodes. First, we can notice that the x-displacement is absorbed in the PML domains with a $1e4$ factor. Indeed, we really pay attention to the validity domain and thus the PML actually acts as a propagation towards the infinity in the same material that initially. Secondly, we can also note the presence of lobes on the left and the right parts of the resonator due to its finite lateral dimension. We already signified the lateral absorbed ones in the PML. However, there are two other which propagate in the y-direction. They are not only absorbed by PML too but also not reflected at the BEM interface indicating thus that the Green radiation conditions work well too. These results show the possibility of combining these two boundary conditions.

5. Conclusions

In this paper, we first demonstrated the theoretical and numerical basis of FEA. We next illustrated the state of the art in simulation based on FEA for 2D and 3D acoustic devices (especially SAW resonators). These examples introduced how the last research in acoustic research needs further improvements of the numerical tools. For instance, the wide and finite SAW resonators cannot be well numerically understood without a new theoretical approach. We drew these numerical improvement based on a finite FEA combining with two different kind of boundary conditions i.e. the PML method and BEM. At last, we show the efficiency of these approach for several example and more precisely we also demonstrated that we can use simultaneously the two boundary conditions to allow the simulation of realistic resonators e.g. we can consider the numerical aperture of an acoustic device.

So we introduced here a new complete numerical based on FEA combining with PML and BEM. We thus are capable to simulate a wide spectrum of resonators. We can simulate periodic as well as non periodic devices. Moreover, new parameters can be considered e.g. aperture or number of electrodes (for SAW resonators). In other worlds, we have now a strong and efficient numerical tool allowing the simulation of nearly all the configurations for SAW and BAW resonators.

Author details

T. Laroche and S. Ballandras
FEMTO-ST institute, Time & Frequency departement, France

6. References

[1] Tobolka, G.: Mixed matrix representation of SAW transducers, IEEE Transactions on Sonics and Ultrasonics 26(6), pp426-428, 1979

[2] Kubat, F., Ruile, W., Rosler, U., Reindl, L.M.: A numerical method for calculating the dynamic stress in SAW devices, Microelectronic Engineering 82(3-4, SI), 670-674, DEC 2005, European Workshop on Materials for Advanced Metalization, Dresden, Germany, 06-09, 2005

[3] Hermelin, D., Daniaux, W., Ballandras, S., Belgacem, B.: Fabrication of Surface Acoustic Wave wireless pressure sensor, 2009 Joint meeting of the European frequency and time forum and the IEEE International Frequency Control Symposium, VOLS 1 and 2, pp96-99, 2009,

[4] Ballandras, S., Wilm, M., Edoa, P.F., Soufyane, A., Laude, V., Steichen, W., Lardat, R.: Finite-element analysis of periodic piezoelectric transducers, Journal of Applied Physics 93(1), pp702-711, JAN 1 2003

[5] Wilm, M., Ballandras, S., Reinhardt, A., Laude, V., Lardat, R., Armati, R., Daniau, W., Lanteri, F., Gelly, J.F., Burat, O.: 3-D mixed finite-element/boundary-element model for the simulation of periodic ultrasound transducers radiating in layered media, 2003 IEEE Ultrasonics Symposium Proceedings, VOLS 1 and 2, 1654-1657

[6] Wang, W.B., Zhang, X.D., Shui, Y.G., Wu, H.D., Zhang, D., Plessky, V.P.: Minimizing the bulk-wave scattering loss in dual-mode SAW devices, IEEE Transactions on Ultrasonics Ferroelectrics and Frequency Control 53(1), 193-198, JAN 2006

[7] Ballandras, S., Laude, V., Pastureaud, T., Wilm, M., Daniau, W., Reinhardt, A., Steichen, W., Lardat, R.: A FEA/BEM approach to simulate complex electrode structures devoted to guided elastic wave periodic transducers, 2002 IEEE Ultrasonics Symposium Proceedings, VOLS 1 and 2, 321-324, Eds: Yuhas, DE and Schneider, SC, 2002, IEEE International Ultrasonic Symposium, MUNICH, GERMANY, OCT 08-11, 2002
[8] Wilm, M., Ballandras, S., Laude, V.: Non periodic acoustic devices radiating in semi-infinite solids simulated by a combination of finite element analysis and a boundary element method, 2004 IEEE Ultrasonics Symposium, Vols 1-3, 1620-1623, Eds: Yuhas, MP, 2004, IEEE Ultrasonics Symposium, Montreal, CANADA, AUG 23-27, 2004
[9] Pastureaud, T., Daniau, W., Laude, V., Wilm, M., Malecamp, Y., Ballandras, S.: Characterization and prediction of transverse plate resonators built using mixed strip and groove gratings, 2001 IEEE Ultrasonics Symposium Proceedings, VOLS 1 and 2, 93-96, Eds: Yuhas, DE and Schneider, SC, 2001, IEEE International Ultrasonic Symposium, ATLANTA, GA, OCT 07-10, 2001
[10] Tiersten, H.F., Hamilton's principle for linear piezoelectric media, Proc. of the IEEE, Vol. 55, pp. 1523- 1524, 1967.
[11] Courant, R., Hilbert, D.: Methods of Mathematical Physics, Interscience Publishers, Inc., 1953
[12] Zienkiewicz, O. C., Taylor, R. L., Zhu, J. Z.: The finite element method: its basis and fundamentals, Butterworth-Heinemann, 2005
[13] Eernisse, E.P., Variational method for electro-elastic vibration analysis, IEEE Transactions on Sonics and Ultrasonics, SU-14, pp. 153-160, 1967.
[14] Clatot, S., Laude, V., Reinhardt, A., Wilm, M., Daniau, W., Ballandras, S., Lardat, R., Solal, M.: Sensitivity of interface acoustic waves to the nature of the interface, 2003 IEEE Ultrasonics Symposium Proceedings, VOLS 1 and 2, 2126-2129, Eds: Yuhas, DE and Schneider, SC, 2003, IEEE International Ultrasonics Symposium, Honolulu, HI, OCT 05-08, 2003
[15] Ballandras, S., Lardat, R., Wilm, M., Pastureaud, Th., Reinhardt, A., Champavert, N., Steichen, W., Daniau, W.; Laude, V., Armati, R., Martin, G., A mixed finite element/boundary element approach to simulate complex guided elastic wave periodic transducers, Journal of Applied Physics, pp014911, 105, 2009.
[16] Daniau, W., Ballandras, B., Briot, J.B., Proceeding of the IEEE International Frequency Control Symposium, pp. 800-806, 1997
[17] Daniau, W., Baron, T., Garcia, J., Laroche, T., Ballandras, S., A 2D Transducer Structure for the Excitation of Surface Acoustic Wave, EFTF 2010, 24th European Frequency and Time Forum, April 2010
[18] Mayer, M., Zaglmayr, S., Wagner, K.,Schöberl, J., Perfectly Matched Layer Finite Element Simulation of Parasitic Acoustic Wave Radiation in Microacoustic Devices, 2007 IEEE Ultrasonics Symposium Proceedings
[19] Tajic, A., Volatier, A., Aigner, R., Solal, M., Simulation of Solidly Mounted BAW Resonators using FEM combined with BEM and/or PML, 2010 IEEE International Ultrasonics Symposium Proceedings
[20] Laroche, T., Ballandras, S., Daniau, W., Garcia, J., Dbich, K., Mayer, M., Perois, X., Wagner, K., Mixed finite element analysis/boundary element method based on canonical Green's function to address non periodic acoustic devices., International Ultrasonics Symposium, 2011

[21] Ventura, P.,Hodé, J.M., Solal, M., Desbois, J. Ribbe, J., Numerical methods for SAW propagation characterization, Proc. of the IEEE Ultrasonics Symposium, pp175-186, 1998.
[22] Hodé, J.M., Desbois, J., Original basic properties of the Green's functions of a semi-infinite piezoelectric substrate, Proc. of the IEEE Ultrasonics Symposium, pp131-136, 1999.
[23] Boyer, L., Étude des phénomènes de réflexion/réfraction dóndes planes acoustiques dans les milieux piézoélectriques, Thèse de lÚniversité de Paris VII an Acoustique Physique, Paris, 1994
[24] Ribbe, J., On the coupling of integral equations and finite element/Fourier modes for the simulation of piezoelectric surface wave component, Phd Thesis, École Polytechnique, 2002.
[25] Berenger, J.P., Three-dimensional perfectly matched layer for the absorption of electromagnetic waves, J. Comp. Phy. 127, 363–79, 1996
[26] Laroche, T., Baida, F.I., Van Labeke, D., Three -dimensional finite-difference time domain study of enhanced second-harmonic generation at the end of a apertureless scanning near-field optical microscope metal tip, josab 22, 1045–1051, 2005
[27] Zheng, Y., Huang, X., Anisotropic Perfectly Matched Layers for Elastic Waves in Cartesian and Curvilinear Coordinates, 2002 MIT Earth Resources Laboratory Industry Consortium Report